Journal of Materials Chemistry A

Accepted Manuscript

ROYAL SOCIETY OF CHEMISTRY

www.rsc.org/materialsA

Capture and electrochemical conversion of CO_2 to ultrathin graphite sheets in $CaCl_2$-based melts

Liwen Hu, Yang Song, Jianbang Ge, Jun Zhu, Shuqiang Jiao*

State Key Laboratory of Advanced Metallurgy, University of Science and Technology Beijing, Beijing, 100083, PR China.

* Corresponding author: sjiao@ustb.edu.cn (S Jiao)

Abstract

Molten $CaCl_2$ has been reported to be potential dopants to reactivate CaO and enhance the cyclic capture ability of CaO. In the present work, the results showed that O^{2-} in molten $CaCl_2$-CaO has a strong affinity for CO_2 at 850℃, where carbonates formed. With the utilization of a RuO_2•TiO_2 inert anode, the formed carbonates are successfully electrochemical split into value-added ultrathin graphite sheets which look like kind of graphene accompanied by the evolution of carbon monoxide at the cathode and environmentally friendly by-product oxygen at the anode. The reduction mechanism of CO_3^{2-} was investigated by cyclic voltammetry and square wave voltammetry. The results demonstrates that two steps are involved during the electrochemical reduction of CO_3^{2-}, and the transferred electron number calculated for each step is 1.76 and 1.99, respectively. The kind of graphene generated at the cathode may have potential applications in various fields such as energy storage and electronic devices. The molten $CaCl_2$-CaO showed potential applications and prospects in large scale capture of CO_2, and the electrochemical conversion of CO_2 into high value added carbon material such as ultrathin graphite sheets with

renewable energy sources.

1. Introduction

Higher demands for energy and materials lead to a greater amount of CO_2 emissions, which is a serious problem for the establishment of a sustainable society and is contrary to the green chemistry concepts.[1-4] The CO_2 emission is considered to be a primary factor in global climate change.[5-8] Various approaches have been proposed for tackling the CO_2 emission ranging from reduction of emission, a change to renewable energy sources,[9-11] and methods to safely capture and store carbon dioxide.[12-14] However, to reduce the CO_2 emission by cutting the utilization of fossil fuels cannot be realized for the next decades because fossil fuels cannot be completely replaced and will still play a dominant role in the energy industry. So the developments of efficient and cost-effective methods for the capture and storage (CCS) along with the conversion (CCC) as well as utilization of CO_2 have been considered to be the best method among the proposed technologies.[15-17] Three of the leading options for large scale CO_2 capture include solvent-based chemisorption techniques, carbonate looping technology, and the so-called oxyfuel process.[18] The transformations are divided into six categories including:[19] (1) chemical transformation of CO_2 to hydrogenated materials (hydrocarbons, MeOH, EtOH, etc.), (2) photochemical transformation to CO, HCO_2H, CH_4, (3) electrochemical/photoelectrochemical transformation to CO, HCO_2H, MeOH and C, (4) biological transformation to EtOH, sugar, CH_3CO_2H, and (5) reforming CO_2 to generate CO and H_2.

Among the various conversion processes, the electrochemical reduction of carbon dioxide to carbon based products are more favorable as the reaction is easy to control and the products are environmentally friendly energy source.[20-22] The electrochemical reduction of carbon dioxide to carbon can be involved in aqueous solutions, ionic liquids and molten salt.[23-25] However, the gas solubility in the aqueous solution is low and the electro-reduction potential of CO_2 is very close to that of water decomposition, which limits the practical electrochemical transformation of CO_2 in aqueous solution.[26, 27] As for ionic liquids, although they owe a wide electrochemical window, high solubility of CO_2 and the product yield reported is higher than that in aqueous solution, the current high cost of RTILs still restricted their widespread applications.[28] Molten salts are considered to be a potential electrolyte for the capture and electrochemical conversion of the carbon dioxide for low cost, high ionic conductivity and the by-products are value-added carbonaceous material and environmentally friendly oxygen.[29-31] Most previous studies are carried out in molten alkali carbonate or molten chlorides and fluorides containing alkali carbonate in which the capture of CO_2 is achieved by the generated O^{2-} produced by electrochemical decomposition of CO_3^{2-} ions.[32-34] Ingram et al. reported cathodic deposition of carbon in molten alkali carbonate in 1966, and Yin et al. proposed the capture and electrochemical conversion of CO_2 with the utilization of renewable energy sources in molten Li-Na-K carbonates by using a Ni cathode and a SnO_2 anode.[16, 35] The deposition of carbon was also achieved in LiCl–KCl–K_2CO_3 and LiF–NaF–Na_2CO_3 melts respectively.[36, 37] Otake et al demonstrated the decomposition of

CO_2 to carbon by the electrochemically reduced Ca or Li in $CaCl_2$-CaO and LiCl-Li_2O melt.[38] However, a relative high cell voltage was needed by using a ZrO_2 solid electrolyte anode, the product in the melt was hard to be collected or may even lead to a short circuit after long-time electrolysis. Therefore, a more efficient and convenient way to the capture and electrochemical conversion of CO_2 at the interface of electrode is proposed and systematically investigated. $CaCl_2$ was considered to be a potential electrolyte for high solubility of oxygen ions which was regarded as the capture agent. Furthermore, $CaCl_2$ has been reported as dopants to reactivate CaO and enhance the long-term reactivity.[39] In the present work, a novel process was proposed for the capture and electrochemical conversion of CO_2 into high value-added and chemical stable carbonaceous material in the molten $CaCl_2$-CaO at 850 ◎. With the utilization of RuO_2•TiO_2 inert anode, the only by-product is environmentally friendly gas of oxygen. Unlike the reported capture process of CO_2 in alkali carbonate, the process proposed herein captures the CO_2 with dissolved oxygen ions directly and electrochemically converted into value-added ultrathin graphite sheet. Compared with all these reported methods, the proposed way herein is more facile and with the utilization of renewable energy sources such as solar and wind, the process can be a potential and significant alternative for the capture and electrochemical conversion of carbon dioxide into graphite sheet in a large scale. Moreover, the process mechanism was systematically investigated by cyclic voltammetry and square wave voltammetry.

2. Experimental

Anhydrous $CaCl_2$ was of analytical purity which was purchased from Sinopharm Chemical Reagent Co., Ltd. The CaO was obtained by calcinating of $CaCO_3$ at 1423K for 15 min. The RuO_2•TiO_2 anode was prepared by mixing TiO_2 and RuO_2 powder in a mortar with mole ratio of 3:7 and was then pressed into pellets with a diameter of 20 mm, using a uniaxial pressure of 3.18 MPa, which were then fired at 950 ◎ for 12h in a muffle furnace. Holes were then drilled in the pellets and platinum wires were then inserted to form the anode. The stainless steel rod and tungsten wire were used as working electrode during electrolysis and electrochemical tests, respectively.

Approximately 200 g anhydrous $CaCl_2$ was added into an alumina crucible, which was placed in a sealed vertical tubular reactor. The salt was dried at 300 ◎ under vacuum for up to 12 h to remove moisture before it was slowly heated up to 850 ◎.

Cyclic voltammetry and square wave voltammetry were performed on an electrochemical workstation (Prinston potentiostat/ galvanostat Model 263 controlled with the powersuite software package) using a three electrode configuration. The prepared TiO_2•RuO_2 anode and tungsten wire (0.04mm in diameter and 0.03896 cm^2 in area) were used as counter electrode and working electrode, respectively. The Ag/AgCl was served as the reference electrode. For square wave voltammetry, the potential–current curve has a Gaussian shape with a peak at a potential close to the half-wave potential for the ionized species. The mathematical expression has the following characteristics:

a) The width of the peak ($W_{1/2}$) at half of its height depends on the number of electrons (n) exchanged at the operating temperature.

$$W_{1/2} = 3.52\frac{RT}{nF} \quad (1)$$

Where R is the ideal gas constant; T: absolute temperature; F: Faraday constant and 3.52 is dimensionless.

b) The peak current (i_P) varies linearly with the concentration of the electroactive species and with the square root of the frequency (f) according to the equation.

$$i_p = nFAC_0\frac{1-\Gamma}{1+\Gamma}\sqrt{\frac{Df}{\pi}} \quad \Gamma = \exp(\frac{nF\Delta E}{2RT}) \quad (2)$$

Where i_P is the peak current, A; n the electron charged number; F the Faraday constant, C; A the electrode area, cm^2; C_0 the concentration of CO_3^{2-} ion, mol/cm^3; D the diffusion coefficient, $cm^2 \cdot s^{-1}$; f the scanning frequency, Hz; R the ideal gas constant, $J \cdot mol^{-1} \cdot K^{-1}$; T temperature, K; ΔE square wave amplitude, V.

Constant cell voltage electrolysis was carried out between $TiO_2 \bullet RuO_2$ anode and stainless steel cathode in molten $CaCl_2$-CaO with the utilization of power supply (Solatron 1287). Before electrolysis experiment, CO_2 was continuously bubbled into the melt through an alumina tube for half an hour and the atmosphere of CO_2 was maintained over the melt continuously. During the electrolysis, the effluent gas from the reactor was monitored with a high-resolution mass spectrometer (Hidden, SPR-30). Prior to off-gas analysis, the reactor was evacuated, and then a testing baseline was established by CO_2. After electrolysis, argon was injected instead of CO_2 and the electrodes were withdrawn to the upper cooler part of the reactor. The cathodic product was taken out and immersed into 1-7 $mol \bullet L^{-1}$ HCl solution to remove the residuals or impurities, and then dried in a drying oven at 120℃.

The obtained products on the cathode were characterized by scanning electron microscopy(SEM, JEOL-JSM-6701F), transmission electron microscopy(TEM, JEOL, JEM-2010) and high-resolution Raman spectroscopic analysis (Horiba-labram HR evolution) with excitation at 532 nm.

Results and discussion

The capture of CO_2 and formation process of CO_3^{2-} in molten $CaCl_2$-CaO was investigated by recording the variation of the current density before and after the injection of CO_2 during the electrolysis. A constant cell voltage of 2.6 V was applied and the result was presented in **Fig. 1**. It can be observed that the measured background current density is only 0.15A•cm^{-2} before the injection of CO_2. Then after the injection of CO_2 into the melt, the current increases quickly due to the rapid dissolution of CO_2 and the formation of CO_3^{2-} between injected CO_2 and the oxygen ions in $CaCl_2$-CaO, resulting in an increasing concentration of CO_3^{2-}. The CO_3^{2-} can be easily electrochemical reduced to carbon and carbon monoxide at the cathode which makes the current density increase quickly. After stopping the injection of CO_2, the measured current density decreases slowly and shows a sustained downward trend due to the continuous consumption of CO_3^{2-} in the melt. The results indicates that the oxygen ions in the melt have a strong affinity for CO_2 even when CO_2 is injected over the melt, which proved the molten $CaCl_2$ is an appropriate capture and electrochemical conversion medium for CO_2. And the carrying capacity for the dissolved CaO in molten $CaCl_2$ was calculated to be about 0.5 g/g of CaO by measuring the mass change of the melt after CO_2 was bubbled into the melt.

Therefore, electrolysis experiments of 4 hours in molten $CaCl_2$-CaO at 850℃ in a two electrode mode was further conducted for investigating electrochemical conversion process of CO_3^{2-} at the stainless steel cathode. Before electrolysis, CO_2 was bubbled into the melt for about half an hour and then maintained over the melt during the electrolysis. The variation of effluent gas from the reactor during the electrolysis was monitored with a high-resolution mass spectrometer, and the results are shown in **Fig.2**. As can be observed, the current-time plot presents that the current increases slowly to a peak of about 1.1A•cm^{-2} during the first 1.5 hours for the fast nucleation of carbon resulting in the increase in surface area of the cathode and the decrease in the over-potential. Thereafter, the current lowers slightly to a steady value of about 1.05A•cm^{-2} due to the continuous consumption of CO_3^{2-} resulting in the reduction in its concentration. Then the current has a steady value which indicates the balance between the consumption of CO_3^{2-} and the capture of CO_2 has been established. The unsmooth current-time pattern can be ascribed to the generation of CO at the cathode during the electrolysis. This can be further proved by the pattern of variation of CO partial pressure, which has the same trend with current versus time profile. Furthermore, the variation of oxygen partial pressure is resembled to the trend of the analogous current versus time profile. The oxygen was generated at the anode by the following reaction:

Anode: $$2CO_3^{2-} - 4e \rightarrow 2CO_2 + O_2 \quad (3)$$

$$2O^{2-} - 4e \rightarrow O_2 \quad (4)$$

After electrolysis, the anode and cathode were both taken out and the photos are

shown in **Fig.3**. As being presented in **Fig. 3b**, the RuO_2•TiO_2 inert anode shows nearly no obvious change in shape and dimension after 4h electrolysis compared with that before electrolysis (Seen in **Fig. 3a**). Furthermore, it can be observed in **Fig. 3c** that the cathode after 4h electrolysis is covered with a thick layer of porous carbon, which indicates that the deposited carbon can serve as a conductive substrate for further growth of carbon. Thereafter, the deposit was peeled off, washed with dilute hydrochloric acid, dried at 120 ◎ for hours and weighted. The graphite yield is calculated to be about 78% after 1 hour electrolysis and will decrease with longer-time electrolysis due to the boudouard reaction. Considering that the graphite yield can be improved by decreasing the temperature and electro-deposition under higher cell voltage with shorter time. Likewise, the photo of the melt is shown in Fig. 3d, from which, it is observed that the melt after electrolysis is quite clean, indicating the reaction is mostly enabled at the surface of electrode. Therefore, FESEM and TEM were further used to characterize the cathodic product.

From the FESEM image in **Fig.4a**, it can be seen the aggregates of carbon particles are in nanosize and random distribution. In **Fig.4b**, it is observed that the multi-walled carbon nanotubes are obtained during electrolysis. The formation of multi-walled carbon nanotubes was obtained after the stainless steel cathode covered with a thick layer of carbon. The observation is further proved by the TEM images. Interestingly, the aggregates are made up of many ultrathin graphite sheets which are transparent and look like kind of graphene and the multi-walled carbon nanotube is 20 nm in diameter. The HRTEM image in **Fig. 4e and Fig. 4f** confirms the graphite sheets

consist of about one to five layers and the carbon nanotube are distorted.

The ultrathin graphite was further characterized by Raman spectrum, and the result is demonstrated in **Fig. 5**. The spectra indicates few/many layers graphene features where a large G band at 1585 cm^{-1} and a large symmetrical 2D band at about 2695 cm^{-1} due to the in-plane vibrational (E2g) mode and the two phonon intervalley double resonance scattering, respectively. A relative small peak can also be observed at the D band (1350 cm-1), which represents defects in the sp^2 lattice.[40]

The above mentioned results demonstrate that CO_2 can be successfully captured and electrochemically converted to carbon and carbon monoxide. Thereafter, the electrochemical conversion mechanism of CO_3^{2-} in molten $CaCl_2$ was investigated by cyclic voltammograms with a tungsten wire being the working electrode at 850◎. To prevent CO_2 from influencing the results, all the electrochemical tests were carried out under an argon atmosphere. The experimental setup is shown in **Fig.6a**. Besides a tungsten wire used as working electrode, the RuO_2•TiO_2 pellet and Ag/AgCl were counter electrode and reference electrode, respectively. The cyclic voltammogram performed in a blank $CaCl_2$ melt is presented by the black line in **Fig. 6b** at the scan rate of 250 mV•s^{-1}. During the scan toward negative potentials, no reduced peak is observed before the generation of liquid calcium (cathodic limit), which indicates that tungsten is stable in the short time during the electrochemical test. Apparently, there is no significant side reactions associated with the redox of electrolyte components as well as the W electrode material in the range from 0.5 V (vs. Ag/AgCl) to -1.3 V (vs. Ag/AgCl). Therefore, credible test results can be achieved within limits.

To further investigate the electrochemical behavior of CO_3^{2-} in $CaCl_2$ melt, CO_3^{2-} was introduced by the addition of $CaCO_3$, cyclic voltammogram of a broader scan range was also performed at the scan rate of 250 mV•s^{-1} and the corresponding result is shown in **Fig. 6c**. A pair of redox peak can be observed in the potential range of -0.6 V- 0 V after the addition of $CaCO_3$. Then the detailed pattern in this potential range is shown inset. It is observed the onset reduction potential for CO_3^{2-} ion is about -0.15(vs. Ag/AgCl) and a broad wave at about -0.45 V (vs. Ag/AgCl) which is attributed to the reduction of carbonate ions, evolution of carbon monoxide or CO_2^{2-} and deposit of carbon can clearly be seen. During positive scan, the relevant oxidation peaks of O is observed, which are corresponding to the oxidation of the deposited carbon. The reduction peaks for the generation of carbon and CO are hard to distinguish for the theoretical dissociation potential for CO_3^{2-} to carbon is 1.066 V(vs. CO_3^{2-}/ CO_2-O_2) and approximate value of 1.012 V(vs. CO_3^{2-}/CO_2-O_2) for CO_3^{2-} to carbon monoxide respectively at 850 ◎. Moreover, cyclic voltammograms of carbonate ions in $CaCl_2$ melt are recorded at various potential scan rates, which are shown in **Fig.6d**. There is a slight peak shift toward the negative direction for a cathodic reaction and toward the positive direction for an anodic reaction with an increase in the scan rates, revealing a quasi-reversible or irreversible process are involved.

Potentiostatic electrolysis was carried out at the potential of -0.5 V (vs. Ag/AgCl) in the three-electrode mode to prove the feasibility for the conversion of carbonate ions into carbon. The current–time plot is shown in **Fig.7a**, the current has an initial

increase followed by steady trend during 1h electrolysis. The initial fast increase in current is likely due to the nucleation of carbon on the cathode and the increase in surface area. The inset picture in **Fig.7a** shows a photograph of the cathode after electrolysis. It is observed that the cathode was covered by a layer of black power. Then the washed product was characterized by Raman. The Raman spectra in **Fig.7b** shows the characteristic peaks of active carbon materials, G band at 1580 cm^{-1} and D band at 1370 cm^{-1}. So it is sure that the reduction peak at -0.45 V can be ascribed to the reduction of carbonate ions.

Furthermore, square wave voltammograms are employed to further illustrate the electrochemical reduction process of CO_3^{2-}. A typical square wave voltammogram at 850 ◎ in molten salt is shown in **Fig. 8a**.Two reduction peaks can be fitted during potential negative sweep. By measuring the width at mid height of each peak and calculating with using Eq. 1, which has been described in detail in the experiment section. The exchanged electron number (n) for each peak is calculated to be:

Peak (R1): n = 1.76

Peak (R2): n = 1.99

The results indicate that two steps are involved during the reduction of CO_3^{2-} and deposit of carbon, in which the R1 peak is related to the soluble–soluble system CO_3^{2-}/ CO_2^{2-} and CO_3^{2-}/ CO and (R2) is associated with the formation of carbon from CO_2^{2-}. Therefore, the reduction process can be concluded as follows:[41]

$$R1:\ CO_3^{2-} + 2e^- \rightarrow CO_2^{2-} + O^{2-} \quad (5)$$

$$CO_3^{2-} + 2e^- \rightarrow CO + 2O^{2-} \quad (6)$$

$$R2:\ CO_2^{2-} + 2e^- \rightarrow C + 2O^{2-} \quad (7)$$

Then square wave voltammograms of different frequencies are fitted and shown in the **Fig.8b**. It indicates the peak current density is proportional to the frequency of a square wave signal and the reduction peak shift towards the negative direction with the increase of frequency which is in accordance with the results of CV. **Fig.8c** shows the fitted peak R1 at different frequencies. The peak current density is increasing regarding to the increase of the scan frequency, According to Oster young and Barker, the height of the peak and the square root of frequency indicate the relationship as Eq. (2). The maximum current of the peak (R1) versus the square root of the frequency of the square wave signal presents a linear relationship. The straight line obtained is shown in **Fig.8d,** which confirms that Eq. (2) can be employed in the frequency range studied. The results indicate the electrochemical reaction results in CO_2^{2-} is controlled by semi-infinite linear diffusion and the diffusion coefficient of CO_3^{2-} in $CaCl_2$ melt at 850 ◎ can be calculated as 2.17×10^{-5} cm^2s^{-1}, which has the same order of magnitude but a little lower than the diffusion coefficient of CO_3^{2-} in molten LiF-NaF reported by Massot.[37] The difference between the values can be explained by the temperature and molten salts media effects, which show up in the mass transfer viscosity of CO_3^{2-}.

The above mentioned results illustrate that CO_2 can be captured by oxygen ions in molten $CaCl_2$ and electrochemically converted into ultrathin graphite by a two step process. In this way, this process is of great significance to be extended to dealing with greenhouse gases from industry in large-scale with the utilization of renewable

energy such as solar and wind. The overall scheme is shown in **Fig. 9**. CO_2 emissions from industry after enrichment can be fed into electrolytic cell continuously where they can be captured by the dissolved oxygen ions in the melt to form carbonate ions. Then the carbonate ions can be electrochemically converted to value-added ultrathin graphite sheet and environmentally friendly by-product oxygen. This process shows broad prospect in the establishment of a sustainable word.

3. Conclusions

In this work, a significant way for the capture and efficient electrochemical conversion of CO_2 has been proposed and realized in molten calcium chloride. CaO containing $CaCl_2$ melt has been demonstrated to have a strong affinity and capture ability for CO_2 due to the high solubility of oxygen ions. The results of cyclic voltammetry and square wave voltammetry indicate that the CO_3^{2-} is easy to be reduced with the reduction potential value of -0.45 V (vs. Ag/AgCl) and the CO_3^{2-} can be electrochemically converted to carbon within a two-step process. Moreover, the diffusion coefficient of CO_3^{2-} in $CaCl_2$ melt at 850 ◎ is calculated to be 2.17×10^{-5} cm^2s^{-1}. The results of electrolysis and on-line gas analysis show that both ultrathin carbon sheet and carbon monoxide are produced at the cathode along with the continuous evolution of environmentally friendly oxygen at the RuO_2•TiO_2 inert anode. With the utilization of renewable energy sources such as solar power and wind power, molten $CaCl_2$-CaO has potential applications and prospects in large scale capture and fast electrochemical conversion of CO_2.

Acknowledgements

The authors are grateful to the National Natural Science Foundation of China (No.51322402) and the Fundamental Research Funds for the Central Universities (230201406500005).

Figure caption

Fig.1 The current-time curve recorded under a constant cell voltage of 2.6 V between a stainless steel cathode and RuO_2•TiO_2 inert anode before and after the injection of CO_2

Fig.2 The on-line outlet gas analysis and current-time curve recorded in $CaCl_2$-CaO at 850◎ during 4h electrolysis with the utilization of RuO_2•TiO_2 inert anode.

Fig.3 Photos of RuO_2•TiO_2 inert anode before (a) and after 4h electrolysis (b) (c) photo of the cathode after 4h electrolysis (d) photo of the melt after 4h electrolysis;

Fig.4 TEM images of the deposited carbon obtained at a constant cell voltage of 2.6 V after washing

Fig.5 Raman spectra of the carbon obtained at the cathode after electrolysis

Fig.6 (a) The experimental setup used in this research (b) Cyclic voltammograms of a 0.3 mm W wire electrode at a scan rate of 250 mV•s^{-1} in the molten $CaCl_2$ at 850◎ in the Ar atmosphere (c) in the molten $CaCl_2$-$CaCO_3$ at 850◎(1.4 *wt*.%) (d) Cyclic voltammograms at various scan rates in the molten $CaCl_2$ at 850◎

Fig.7 (a) Potentiostatic electrolysis at the potential of -0.5 V (vs. Ag/AgCl) in the three-electrode mode and the inserted picture is a photo of cathode after electrolysis (b) Raman spectra of the carbon obtained at the cathode after electrolysis

Fig.8 (a) A typical square wave voltammogram recorded in molten $CaCl_2$ with 1.4 *wt*.% calcium carbonate. The square wave amplitude was 20 mV, while the frequency was 50 Hz (b) Variation of the square wave voltammograms with the frequency recorded in molten $CaCl_2$ with 1.4 *wt*.% calcium carbonate (c) Variation of fitted reduction peak R1 with the frequency. The square wave amplitude was 20 mV (d) The linear relationship between square wave peak current of R1 and square root of frequency

Fig.9 The capture and electrochemical conversion scheme of CO_2 in molten salt

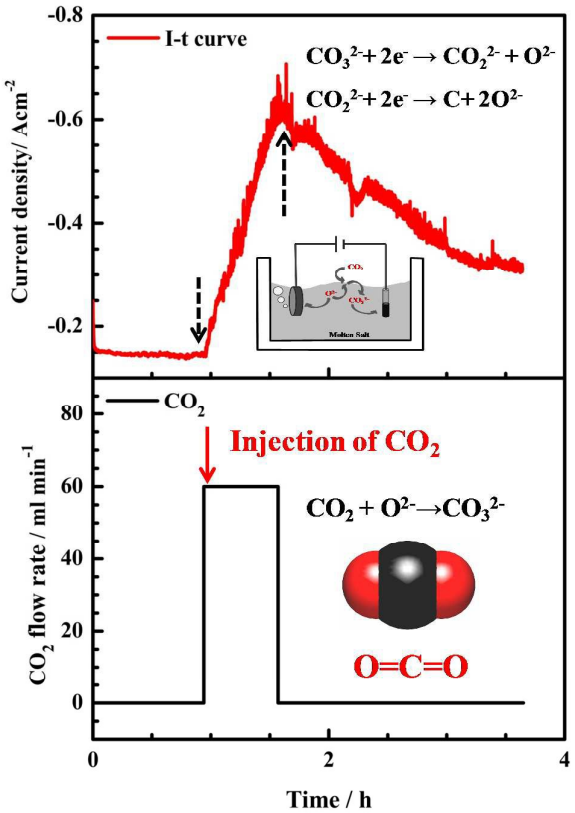

Fig.1

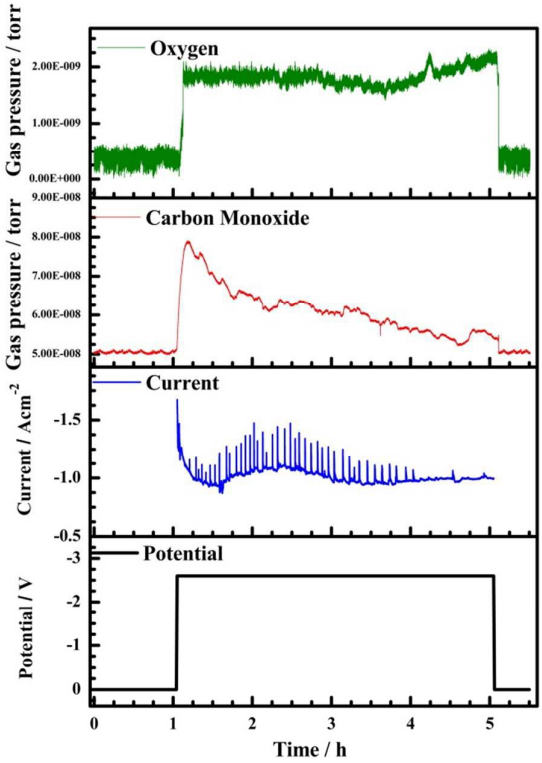

Fig.2

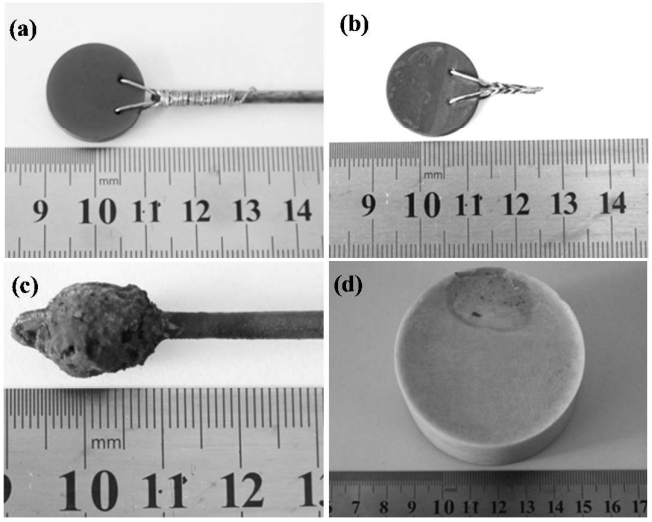

Fig.3

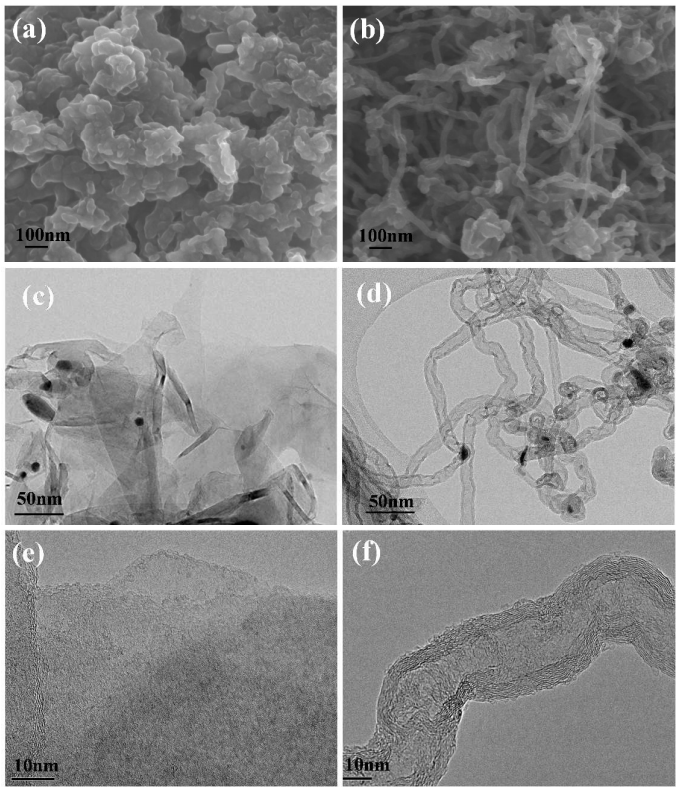

Fig.4

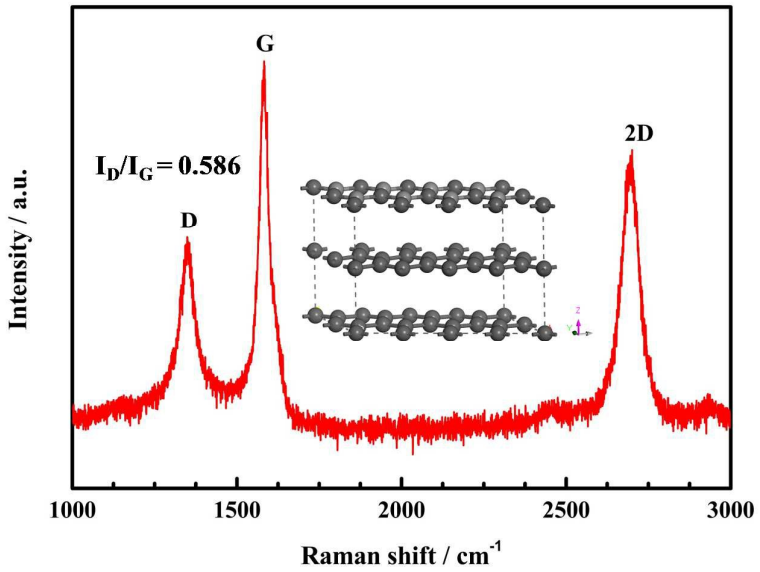

Fig.5

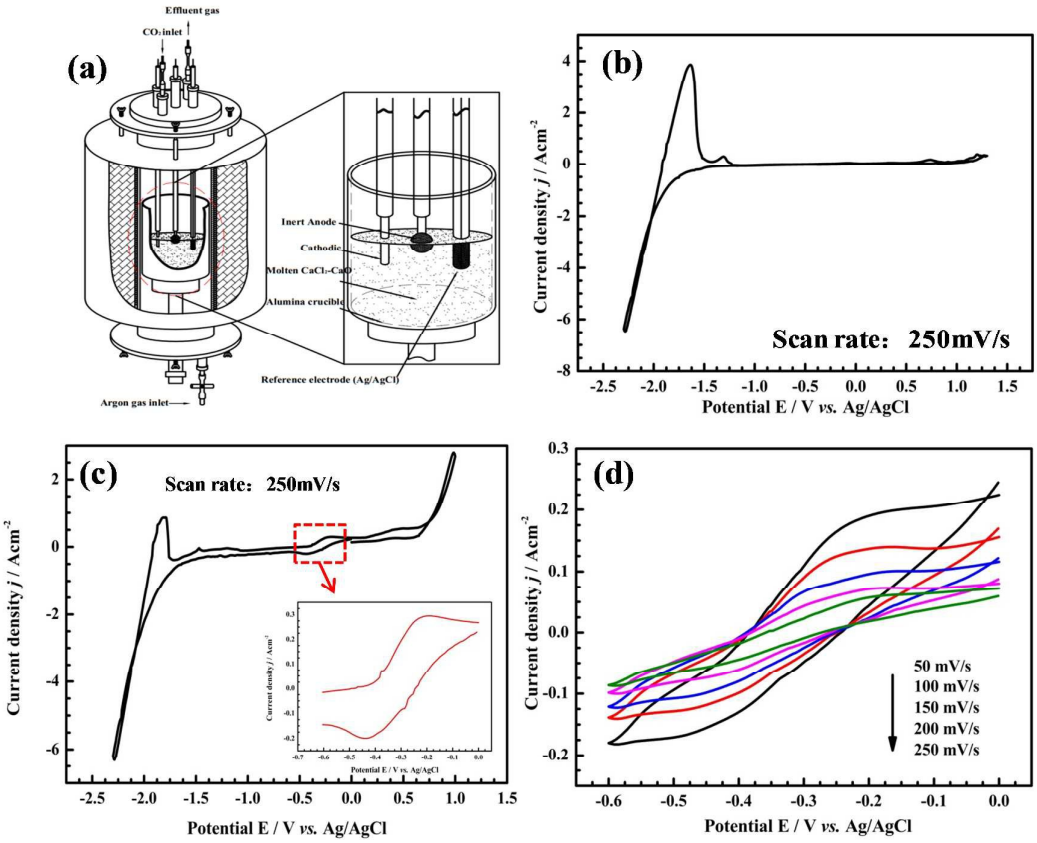

Fig.6

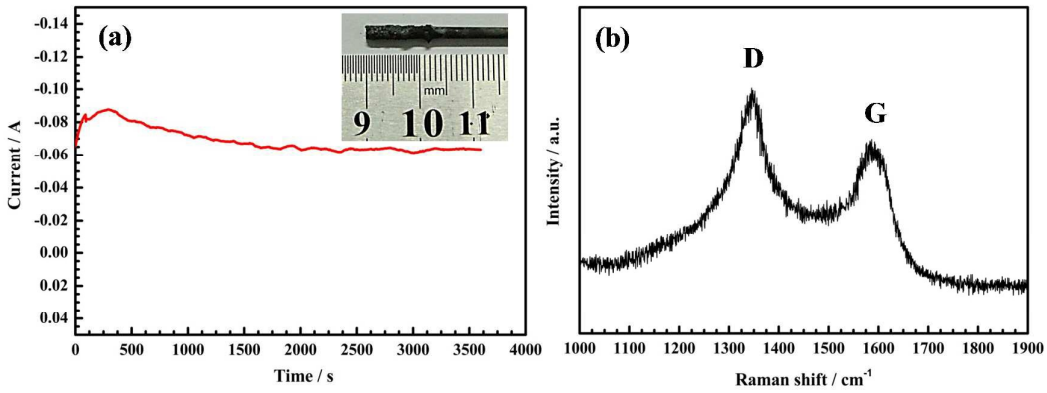

Fig.7

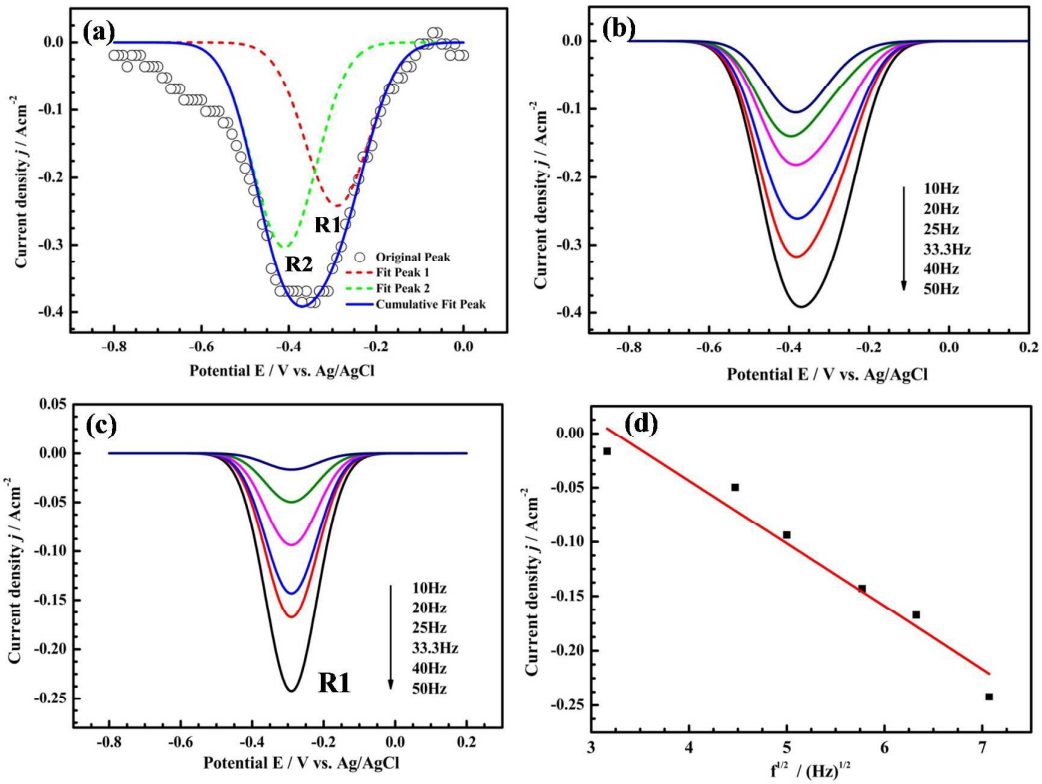

Fig.8

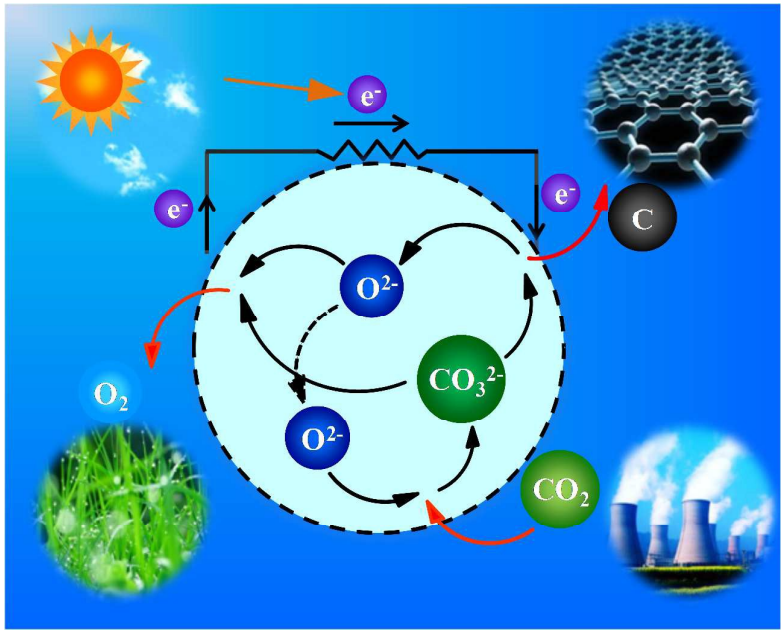

Fig.9

1. H. Arakawa, M. Aresta, J. N. Armor, M. A. Barteau, E. J. Beckman, A. T. Bell, J. E. Bercaw, C. Creutz, E. Dinjus, D. A. Dixon, K. Domen, D. L. DuBois, J. Eckert, E. Fujita, D. H. Gibson, W. A. Goddard, D. W. Goodman, J. Keller, G. J. Kubas, H. H. Kung, J. E. Lyons, L. E. Manzer, T. J. Marks, K. Morokuma, K. M. Nicholas, R. Periana, L. Que, J. Rostrup-Nielson, W. M. Sachtler, L. D. Schmidt, A. Sen, G. A. Somorjai, P. C. Stair, B. R. Stults and W. Tumas, *Chem Rev*, 2001, **101**, 953-996.

2. S. Licht, B. Wang, S. Ghosh, H. Ayub, D. Jiang and J. Ganley, *J. Phys. Chem. Lett.*, 2010, **1**, 2363-2368.

3. Y. Xie, T.-T. Wang, X.-H. Liu, K. Zou and W.-Q. Deng, *Nat Commun*, 2013, **4**.

4. M. García, M. J. Aguirre, G. Canzi, C. P. Kubiak, M. Ohlbaum and M. Isaacs, *Electrochim. Acta*, 2014, **115**, 146-154.

5. C.-H. Yu, C.-H. Huang and C.-S. Tan, *Aerosol. Air. Qual. res*, 2012, **12**, 745-769.

6. P. Zakkour and M. Haines, *International Journal of Greenhouse Gas Control*, 2007, **1**, 94-100.

7. E. S. Rubin, H. Mantripragada, A. Marks, P. Versteeg and J. Kitchin, *Prog. Energ. Combust*, 2012, **38**, 630-671.

8. M. Bourrez, F. Molton, S. Chardon-Noblat and A. Deronzier, *Angew. Chem*, 2011, **123**, 10077-10080.

9. M. Aresta, A. Dibenedetto and A. Angelini, *Philos. Trans. R. Soc. London, Ser. A*, 2013, **371**, 20120111.

10. Y. Taniguchi, H. Yoneyama and H. Tamura, *Bull. Chem. Soc. Jpn.*, 1982, **55**, 2034-2039.

11. I. Ganesh, *Renew. Sust. Energ. Rev.*, 2014, **31**, 221-257.

12. P. Li, B. Ge, S. Zhang, S. Chen, Q. Zhang and Y. Zhao, *Langmuir*, 2008, **24**, 6567-6574.

13. G. H. Rau, *Environ. Sci. Technol.*, 2010, **45**, 1088-1092.

14. P. Karpe and C. P. Aichele, *Environ. Sci. Technol.*, 2013, **47**, 3926-3932.

15. M. Mikkelsen, M. Jørgensen and F. C. Krebs, *Energ. Environ. Sci.*, 2010, **3**, 43-81.

16. H. Yin, X. Mao, D. Tang, W. Xiao, L. Xing, H. Zhu, D. Wang and D. R. Sadoway, *Energ. Environ. Sci.*, 2013, **6**, 1538-1545.

17. J. Ge, L. Hu, W. Wang, H. Jiao and S. Jiao, *ChemElectroChem*, 2015, **2**, 224-230.

18. N. MacDowell, N. Florin, A. Buchard, J. Hallett, A. Galindo, G. Jackson, C. S. Adjiman, C. K. Williams, N. Shah and P. Fennell, *Energ. Environ. Sci.*, 2010, **3**, 1645-1669.

19. T. Sakakura, J.-C. Choi and H. Yasuda, *Chem Rev*, 2007, **107**, 2365-2387.

20. S. Licht, *Adv. Mater.*, 2011, **23**, 5592-5612.

21. S. Sen, D. Liu and G. T. R. Palmore, *ACS. Catal*. 2014, **4**, 3091-3095.

22. M. Karamad, H. A. Hansen, J. Rossmeisl and J. K. Norskov, *ACS. Catal*., 2015.

23. M. Gattrell, N. Gupta and A. Co, *J. Electroanal. Chem.*, 2006, **594**, 1-19.

24. J. E. Bara, D. E. Camper, D. L. Gin and R. D. Noble, *Accounts. Chem. Res.*, 2009, **43**, 152-159.

25. E. D. Bates, R. D. Mayton, I. Ntai and J. H. Davis, *J. Am. Chem. Soc.*, 2002, **124**, 926-927.

26. H. Zhong, K. Fujii, Y. Nakano and F. Jin, *J. Phys. Chem. C.*, 2014, **119**, 55-61.

27. M. Z. Ertem, S. J. Konezny, C. M. Araujo and V. S. Batista, *J.Phys. Chem. Lett.*, 2013, **4**, 745-748.

28. L. Sun, G. K. Ramesha, P. V. Kamat and J. F. Brennecke, *Langmuir*, 2014, **30**, 6302-6308.

29. H. V. Ijije, C. Sun and G. Z. Chen, *Carbon*, 2014, **73**, 163-174.

30. I. A. Novoselova, N. F. Oliinyk, S. V. Volkov, A. A. Konchits, I. B. Yanchuk, V. S. Yefanov, S. P. Kolesnik and M. V. Karpets, *Physica. E*, 2008, **40**, 2231-2237.

31. Lantelme, Frederic, and Henri Groult. *Molten salts chemistry: from lab to applications*. Newnes, 2013

32. B. Kaplan, H. Groult, A. Barhoun, F. Lantelme, T. Nakajima, V. Gupta, S. Komaba and N. Kumagai, *J. Electrochem. Soc.*, 2002, **149**, D72-D78.

33. V. Kaplan, E. Wachtel and I. Lubomirsky, *J. Electrochem. Soc.*, 2014, **161**, F54-F57.

34. B. Kaplan, H. Groult, S. Komaba, N. Kumagai and F. Lantelme, *Chem Lett.*, 2001, 714-715.

35. M. D. Ingram, B. Baron and G. J. Janz, *Electrochim. Acta*, 1966, **11**, 1629-1639.

36. H. Kawamura and Y. Ito, *J. Appl. Electrochem.*, 2000, **30**, 571-574.

37. L. Massot, P. Chamelot, F. Bouyer and P. Taxil, *Electrochim. Acta*, 2002, **47**, 1949-1957.

38. K. Otake, H. Kinoshita, T. Kikuchi and R. O. Suzuki, *Electrochim. Acta*, 2013, **100**, 293-299.

39. V. Tomkute, A. Solheim and E. Olsen, *Energy Fuels*, 2013, **27**, 5373-5379.

40. M. Jaiswal, C. H. Yi Xuan Lim, Q. Bao, C. T. Toh, K. P. Loh and B. Ozyilmaz, *ACS nano*, 2011, **5**, 888-896.

41. H. V. Ijije, R. C. Lawrence and G. Z. Chen, *RSC. Adv.*, 2014, **4**, 35808-35817.

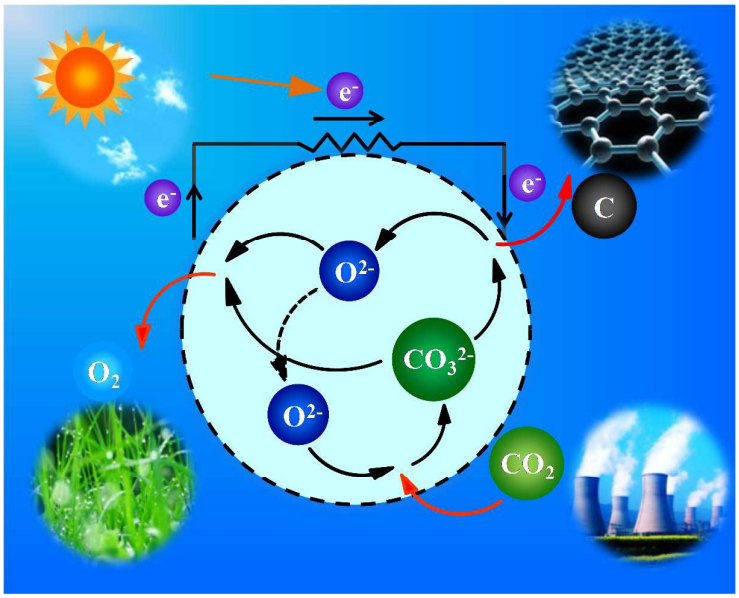

Molten $CaCl_2$ has been demonstrated to be potential dopants to reactivate CaO and enhance the cyclic capture ability of CaO. The results showed O^{2-} in molten calcium chloride has a strong affinity for CO_2 at 850℃, which formed carbonates. With the utilization of a RuO_2•TiO_2 inert anode, the formed carbonates was successfully electrochemical split into value-added ultrathin graphite sheets which look like kind of graphene accompanied by the evolution of carbon monoxide at the cathode and environmentally friendly by-product oxygen at the anode. Then the reduction mechanism of CO_3^{2-} was investigated by cyclic voltammetry and square wave voltammetry. The results demonstrated that two steps are involved during the electrochemical reduction of CO_3^{2-}, the transferred electron number calculated for each step is 1.76 and 1.99 respectively. The kind of graphene generated at the cathode may have potential applications in various fields such as energy storage and electronic devices. The molten $CaCl_2$-CaO showed potential applications and prospects in large scale capture of CO_2, and electrochemical conversion of CO_2 into high value added carbon material such as ultrathin graphite sheets with renewable energy sources.